PHYSICS AND CHEMISTRY OF SOLID STATE

V. 26, No. 3 (2025) pp. 541-548

Section: Physics

DOI: 10.15330/pcss.26.3.541-548

Vasyl Stefanyk Carpathian National University

ФІЗИКА І ХІМІЯ ТВЕРДОГО ТІЛА Т. 26, № 3 (2025) С. 541-548

Фізико-математичні науки

UDC 538.9 ISSN 1729-4428 (Print) ISSN 2309-8589 (Online)

D.M. Chervinko, B.I. Rachii, L.S. Yablon, V.O. Kotsiubynsky, O.P. Pakhovsky, I.M. Hasiuk

Modification of the Dispersion Curve Shape of Liver Tissue Conductivity under the Influence of Destructive Factors

Vasyl Stefanyk Precarpathian National University Department of Applied Physics and Materials Science, Ivano-Frankivsk, Ukraine, <u>ivan.hasiuk@pnu.edu.ua</u>,

This work investigates the frequency dispersion of electrical properties of biological tissues, particularly pig liver, using spectral analysis of conductivity. Numerical differentiation of impedance characteristics was applied over a wide frequency range $(0.01~\mathrm{Hz}-100~\mathrm{kHz})$ to identify local transitions between tissue electrophysiological regimes. It is shown that the position of the local minimum of the first derivative of the imaginary part of specific conductivity near 1 Hz, corresponding to alpha-dispersion and interfacial polarization on cell membranes, remains stable regardless of sample size but shifts sensitively under the influence of destructive factors (e.g., temperature, radiation). These results confirm the feasibility of using conductivity derivatives as an informative marker of structural changes in tissues, complementing classic impedance approaches for diagnosing and monitoring pathological processes.

Keywords: impedance spectroscopy, electrical conductivity dispersion, liver tissues, electrical equivalent circuit, destruction, alpha-dispersion, numerical differentiation, biological tissues, cell membranes.

Received 23 March 2025; Accepted 28 August 2025.

Introduction

Electrical Impedance Spectroscopy (EIS) is an effective method for studying the electrical properties of biological tissues [1, 2], providing a non-invasive assessment of their composition, hydration, and physiological changes [3, 4]. EIS is widely used for differentiating pathological changes in tissues of various organs, particularly the liver [5], and has an advantage over other methods due to its ability to quantitatively assess cellular changes and its wide frequency range [5]. The method allows real-time measurements and is applied for the development of biosensors, as well as the assessment of tissue status in vivo, in vitro, and ex vivo [7, 8].

However, insufficient reproducibility and repeatability of results, caused by material heterogeneity, electrode polarization, and external conditions, especially for complex tissues, is a major problem in applying the method [3, 6, 18]. Factors affecting the reproducibility of

EIS results are divided into structural features of tissues, measurement signal parameters, and methodological aspects. Biological tissues are complex systems with various electrical properties that depend on anisotropy, chemical composition, and physiological state [5, 20]. Properties also depend on the time after tissue removal from the body [19]. The frequency range of measurement is critical, as choosing the wrong range can distort results due to heat generation or electrode polarization [11, 12]. Important methodological aspects include the use of a four-electrode technique, control of contact impedance and electrode cleanliness, and consideration of external conditions [3, 6, 8].

Current research actively applies EIS for diagnosing pathological conditions of the liver, including fibrosis, steatosis, and cancer [7, 19]. However, poor reproducibility of results remains a problem due to electrode polarization, distributed parameters, and simplification of complex tissue models [3, 6, 8, 10]. To address this problem, the development of new electrodes,

improvement of mathematical models, application of machine learning, and inter-laboratory studies are promising. This will allow wider use of EIS in clinical practice and research [22, 23].

In the proposed study, an attempt was made to find parameters of frequency dispersion curves of electrical conductivity of liver tissues that are stable under different measurement conditions and sensitive to structural destructive changes in the tissue caused by various aggressive factors.

I. Materials and Methods

Pig liver tissues were used as a model biological material for obtaining impedance spectra. After slaughter, the animal organ was cooled and kept in a thermostat at +4 °C. The experiment began 5-6 hours after biomaterial collection. Tissue samples were formed in a 2 ml medical syringe plastic body, which served as a measuring cell. Sample dimensions were: base diameter – 10 mm, height - 5-20 mm. Destructive factors chosen for influence were storage in water, thiourea solution, γ -irradiation, exposure to air at room temperature, 5 °C, and 60 °C for 1 hour. Impedance spectra were recorded using an AUTOLAB PGStat 30 spectrometer in the frequency range from 0.01 Hz to 100 kHz. To minimize the influence of electrical voltage on the structure of organic tissues, the amplitude of the measuring signal was limited to the range of 0-5 mV.

Thermostating was performed using a standard thermostat model 1/120 SPU, which ensured stable temperature conditions throughout the experiment. Numerical processing of measurement results, construction of Nyquist diagrams, and data approximation with determination of electrical equivalent circuit parameters were carried out in FRA-2, Z-View 2, and Origin Lab software environments.

II. Results and Discussion

Figure 1 shows the dispersion curves of the real Y'

and imaginary Y" parts of the electrical conductivity of liver tissues after repeated experiments. A gradual increase in the real part of the conductivity with frequency is observed, indicating a decrease in the influence of interfacial boundaries and a weakening of capacitive resistance. The imaginary part shows a maximum in the mid-frequency range, which reflects polarization on cell membranes [14, cite: 42]. Reducing the sample size more clearly reflects the influence of surface effects, which enhances the oscillations of the imaginary component. Repeated measurements indicate the instability of results due to the influence of the forming signal. At the same time, the shape of the curve, which can serve as an indicator of the state of the system under study, is preserved. To characterize the shape of the dispersion curves, an analysis of their derivatives was used.

Since the measurements are performed over a wide frequency range with a logarithmic distribution of selected frequency values, it is rational to use an equivalent circuit of the impedance system containing three seriesconnected R-CPE branches to calculate the derivatives. According to the assumption [14, cite: 45], based on the internal structure of the tissue, R1 and CPE1 describe the conductivity and capacitance of the extracellular medium, R₂-CPE₂ – intracellular pathways, and R₃-CPE₃ membrane structures with a short time constant. Each part of the spectrum is formed mainly due to the corresponding branch: the low-frequency zone reflects polarization at the tissue-electrode interface (R₁-CPE₁), medium frequencies - bulk conductivity (R2-CPE2), high frequencies membrane response (R3-CPE3). According to this system, the complex impedance of the systems is:

1. For one parallel connection of R and CPE:

$$Z(\omega) = \frac{R}{1 + RQ(j\omega)^n}$$

Let's expand the denominator, taking into account that

$$(j\omega)^n = \omega^n \left[\cos\left(\frac{\pi n}{2}\right) + j\sin\left(\frac{\pi n}{2}\right)\right]$$

Then:

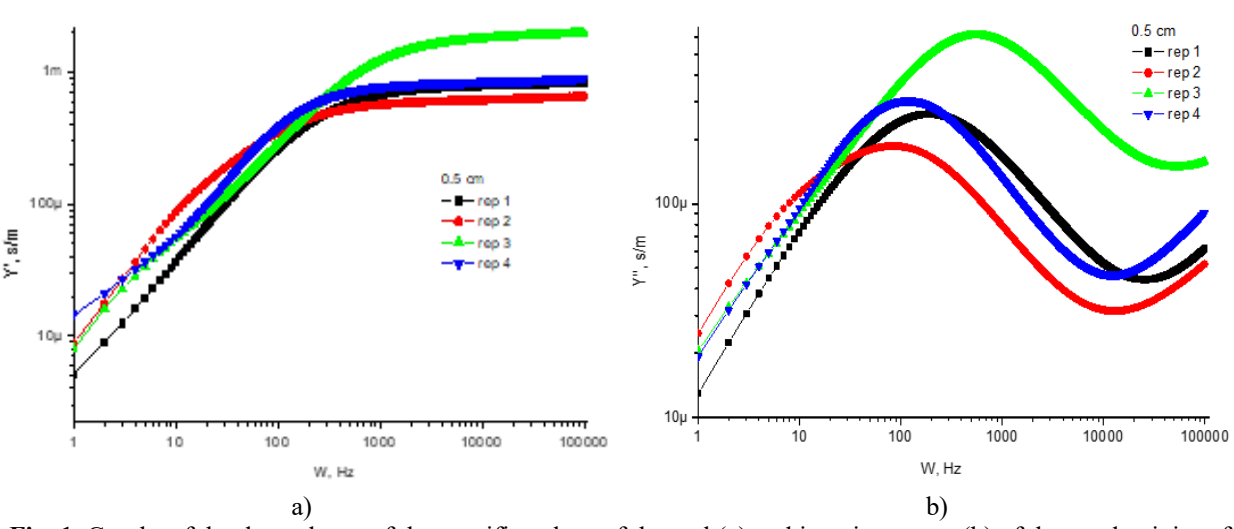


Fig. 1. Graphs of the dependence of the specific values of the real (a) and imaginary part (b) of the conductivity of cylindrical liver samples 0,5 cm high during repeated acquisition of electrical impedance spectra as a function of frequency.

Modification of the Dispersion Curve Shape of Liver Tissue Conductivity under the Influence of Destructive Factors

$$Z(\omega) = \frac{R}{1 + RQ\omega^n \left[\cos\left(\frac{\pi n}{2}\right) + j\sin\left(\frac{\pi n}{2}\right)\right]}$$

Let's write this in standard form:

$$Z(\omega) = \frac{R}{1 + RQ\omega^n \cos\left(\frac{\pi n}{2}\right) + jRQ\omega^n \sin\left(\frac{\pi n}{2}\right)}$$

2. Multiply the numerator and denominator by the conjugate denominator to extract the real and imaginary parts:

$$Z(\omega) = \frac{R\left[1 + RQ\omega^n \cos\left(\frac{\pi n}{2}\right) - jRQ\omega^n \sin\left(\frac{\pi n}{2}\right)\right]}{\left[1 + RQ\omega^n \cos\left(\frac{\pi n}{2}\right)\right]^2 + \left[RQ\omega^n \sin\left(\frac{\pi n}{2}\right)\right]^2}$$

From this, we get:

Real and imaginary parts of a single chain:

$$Z'(\omega) = \frac{R\left[1 + RQ\omega^n \cos\left(\frac{\pi n}{2}\right)\right]}{\left[1 + RQ\omega^n \cos\left(\frac{\pi n}{2}\right)\right]^2 + \left[RQ\omega^n \sin\left(\frac{\pi n}{2}\right)\right]^2}$$

$$Z''(\omega) = -\frac{R_k^2 Q_k \omega^{n_k} \sin\left(\frac{\pi n_k}{2}\right)}{\left[1 + R_k Q_k \omega^{n_k} \cos\left(\frac{\pi n_k}{2}\right)\right]^2 + \left[R_k Q_k \omega^{n_k} \sin\left(\frac{\pi n_k}{2}\right)\right]^2}$$

For the complete circuit consisting of three such series-connected chains, the impedance sums up:

$$Z(\omega) = Z_1(\omega) + Z_2(\omega) + Z_3(\omega)$$

Therefore, the total real and imaginary parts will be the sums of the corresponding parts:

Total real part of the circuit:

$$Z'_{\text{total}}(\omega) = Z'_{1}(\omega) + Z'_{2}(\omega) + Z'_{3}(\omega)$$

Total imaginary part of the circuit:

$$Z_{\text{total}}^{"}(\omega) = Z_1^{"}(\omega) + Z_2^{"}(\omega) + Z_3^{"}(\omega)$$

That is, we substitute the formulas found above for each link with the corresponding parameters obtained from the calculation of the equivalent electrical circuit

For the complete circuit, the real $(Z'(\omega))$ and imaginary $(Z''(\omega))$ parts will look like this:

$$\begin{split} Z'_{total}(\omega) &= \sum_{k=1}^{3} \frac{R_{k} \left[1 + R_{k}Q_{k}\omega^{n_{k}} \cos\left(\frac{\pi n_{k}}{2}\right) \right]}{\left[1 + R_{k}Q_{k}\omega^{n_{k}} \cos\left(\frac{\pi n_{k}}{2}\right) \right]^{2} + \left[R_{k}Q_{k}\omega^{n_{k}} \sin\left(\frac{\pi n_{k}}{2}\right) \right]^{2}} \\ Z''_{total}(\omega) &= -\sum_{k=1}^{3} \frac{R_{k}^{2}Q_{k}\omega^{n_{k}} \sin\left(\frac{\pi n_{k}}{2}\right)}{\left[1 + R_{k}Q_{k}\omega^{n_{k}} \cos\left(\frac{\pi n_{k}}{2}\right) \right]^{2} + \left[R_{k}Q_{k}\omega^{n_{k}} \sin\left(\frac{\pi n_{k}}{2}\right) \right]^{2}} \end{split}$$

where k is the chain number (from 1 to 3).

Let's consider conductivity $Y(\omega)$, which is the inverse of impedance $Z(\omega)$

$$Y(\omega) = \frac{1}{Z(\omega)}$$

Since the circuit consists of three series blocks, each of which is a parallel connection of R and CPE, it is more convenient to first calculate the conductivity of each parallel block, and then obtain the total conductivity of the circuit.

For parallel connected R and CPE:

Resistor conductivity:

$$Y_R = \frac{1}{R}$$

CPE element conductivity:

$$Y_{CPE} = Q(j\omega)^n = Q\omega^n \left[\cos\left(\frac{\pi n}{2}\right) + j\sin\left(\frac{\pi n}{2}\right)\right]$$

Thus, the total conductivity of a single block (parallel connection):

$$Y(\omega) = Y_R + Y_{CPE} = \frac{1}{R} + Q\omega^n \cos\left(\frac{\pi n}{2}\right) + jQ\omega^n \sin\left(\frac{\pi n}{2}\right)$$

From this, we extract the real and imaginary parts of the conductivity of an individual block:

Real part of conductivity of a single block:

$$Y'(\omega) = \frac{1}{R} + Q\omega^n \cos\left(\frac{\pi n}{2}\right)$$

Imaginary part of conductivity of a single block:

$$Y''(\omega) = Q\omega^n \sin\left(\frac{\pi n}{2}\right)$$

For series connection of elements, the circuit conductivity $Y_{\text{total}}(\omega)$ is equal to:

$$\frac{1}{Y_{\text{total}}(\omega)} = \frac{1}{Y_{1}(\omega)} + \frac{1}{Y_{2}(\omega)} + \frac{1}{Y_{3}(\omega)}$$

Or:

$$Y_{\text{total}}(\omega) = \frac{1}{\frac{1}{Y_1(\omega)} + \frac{1}{Y_2(\omega)} + \frac{1}{Y_3(\omega)}}$$

where each individual $Y_k(\omega)$:

$$Y_k(\omega) = \frac{1}{R_k} + Q_k \omega^{n_k} \cos\left(\frac{\pi n_k}{2}\right) + jQ_k \omega^{n_k} \sin\left(\frac{\pi n_k}{2}\right)$$

or convenience of calculations, let's first write the impedances of individual blocks:

$$Z_k(\omega) = \frac{1}{Y_k(\omega)} = \frac{1}{\frac{1}{R_k} + Q_k \omega^{n_k} \cos\left(\frac{\pi n_k}{2}\right) + jQ_k \omega^{n_k} \sin\left(\frac{\pi n_k}{2}\right)}$$

After this, the total impedance of the circuit is simply

the sum (series connection):

$$Z_{total}(\omega) = Z_1(\omega) + Z_2(\omega) + Z_3(\omega)$$

Then the total conductivity of the circuit:

$$Y_{\text{total}}(\omega) = \frac{1}{Z_{\text{total}}(\omega)} = \frac{1}{Z_{1}(\omega) + Z_{2}(\omega) + Z_{3}(\omega)}$$

Let's write the real and imaginary parts of this quantity explicitly:

Real part:

$$Y'_{\text{total}}(\omega) = \frac{z'_{\text{total}}(\omega)}{\left[z'_{\text{total}}(\omega)\right]^2 + \left[z''_{\text{total}}(\omega)\right]^2}$$

Imaginary part:

$$Y_{\text{total}}^{\prime\prime}(\omega) = -\frac{Z_{\text{total}}^{\prime\prime}(\omega)}{\left[Z_{\text{total}}^{\prime}(\omega)\right]^{2} + \left[Z_{\text{total}}^{\prime\prime}(\omega)\right]^{2}}$$

where $Z'_{\text{total}}(\omega)$ and $Z''_{\text{total}}(\omega)$ - are the real and imaginary parts of the total impedance, found in the previous step:

$$Z'_{\text{total}}(\omega) = \sum_{k=1}^{3} \frac{R_k \left[1 + R_k Q_k \omega^{n_k} \cos\left(\frac{\pi n_k}{2}\right) \right]}{\left[1 + R_k Q_k \omega^{n_k} \cos\left(\frac{\pi n_k}{2}\right) \right]^2 + \left[R_k Q_k \omega^{n_k} \sin\left(\frac{\pi n_k}{2}\right) \right]^2}$$

$$Z_{\text{total}}^{\prime\prime}\left(\omega\right) = -\sum_{k=1}^{3} \frac{R_{k}^{2} Q_{k} \omega^{n_{k}} \sin\left(\frac{\pi n_{k}}{2}\right)}{\left[1 + R_{k} Q_{k} \omega^{n_{k}} \cos\left(\frac{\pi n_{k}}{2}\right)\right]^{2} + \left[R_{k} Q_{k} \omega^{n_{k}} \sin\left(\frac{\pi n_{k}}{2}\right)\right]^{2}}$$

Thus, finally:

$$Y_{\text{total}}'\left(\omega\right) = \frac{\sum_{k=1}^{3} \frac{R_{k}\left[1 + R_{k}Q_{k}\omega^{n}k\cos\left(\frac{\pi n_{k}}{2}\right)\right]}{\left[1 + R_{k}Q_{k}\omega^{n}k\cos\left(\frac{\pi n_{k}}{2}\right)\right]^{2} + \left[R_{k}Q_{k}\omega^{n}k\sin\left(\frac{\pi n_{k}}{2}\right)\right]^{2}}}{\left(Z_{\text{total}}'\left(\omega\right)\right)^{2} + \left(Z_{\text{total}}''\left(\omega\right)\right)^{2}}$$

$$Y_{\text{total}}^{\prime\prime}\left(\omega\right) = -\frac{-\sum_{k=1}^{3} \frac{R_{k}^{2} Q_{k} \omega^{n_{k}} \sin\left(\frac{\pi n_{k}}{2}\right)}{\left[1 + R_{k} Q_{k} \omega^{n_{k}} \cos\left(\frac{\pi n_{k}}{2}\right)\right]^{2} + \left[R_{k} Q_{k} \omega^{n_{k}} \sin\left(\frac{\pi n_{k}}{2}\right)\right]^{2}}{\left(Z_{\text{total}}^{\prime}\left(\omega\right)\right)^{2} + \left(Z_{\text{total}}^{\prime\prime}\left(\omega\right)\right)^{2}}$$

Due to the analytical complexity of the complex conductivity formula, the derivatives $\frac{dY'(w)}{dw}$ and $\frac{dY''(w)}{dw}$ were calculated by numerical differentiation over the full frequency range. Figure 2 shows the derivatives of the dispersion curves, and Table 1 shows the positions of the local minima.

Table 1.

Position of local minima of the dy"/dw derivative depending on sample height.

| 5 cm | min, c ⁻¹ | 1 cm | min, c ⁻¹ |
|------------|----------------------|------------|----------------------|
| 1st repeat | 1,11 | 1st repeat | 1,10 |
| 2nd repeat | 0,76 | 2nd repeat | 0,95 |
| 3d repeat | 1,22 | 3d repeat | 0,65 |
| 4th repeat | 0,78 | 4th repeat | 1,27 |
| 1,5 cm | | 2 cm | |
| 1st repeat | 1,2 | 1st repeat | 1,12 |
| 2nd repeat | 1,04 | 2nd repeat | 0,95 |
| 3d repeat | 1,12 | 3d repeat | 0,77 |
| 4th repeat | 1,22 | 4th repeat | 0,96 |

Slight changes in the position of the local minimum of the dy"/dw derivative in samples of the same size between repeated measurements may be due to microstructural rearrangements of the tissue, sensitivity to contact conditions, instability of interfacial polarization, and mathematical features of CPE elements (Table 1). Values above 1 Hz indicate a shift in the system's reactive response to an area of partial smoothing of polarization or blurring of cell boundaries, while values below 1 Hz

reflect classical alpha-dispersion with a dominance of membrane polarization.

Analysis of changes in the first derivative of complex conductivity (Fig. 2) allows for the identification of areas with the most pronounced transitions in current transfer mechanisms. Extremes in the derivatives correspond to frequencies where polarization on cell membranes (alphadispersion) dominates or the structure of conductive pathways changes. For small-sized samples, increased sensitivity to surface effects is observed, leading to a shift and amplification of derivative oscillations, especially in the imaginary part. In addition, repeated measurements could cause variations in humidity, ion diffusion, or partial rearrangement of the cellular architecture, which also affected the shape of the derivative. The obtained data demonstrate that the first derivative is an informative marker of local changes in the electrical behavior of the tissue.

By analogy, let us consider the dispersion curves of the real and imaginary parts of liver tissue conductivity subjected to destructive influences (Fig. 3). In this case, the shape of the dispersion curve, determined by the derivatives $\frac{dY'(w)}{dw}$ and $\frac{dY''(w)}{dw}$, changes significantly. Table 2 presents the general positions of local minima in the low-frequency range, the dispersion in which is determined by α -processes [26]. Alpha-dispersion in biological tissue is a low-frequency electrical dispersion (approximately in the range of 10 Hz – 10 kHz) that arises due to interfacial polarization at the boundary of cell membranes.

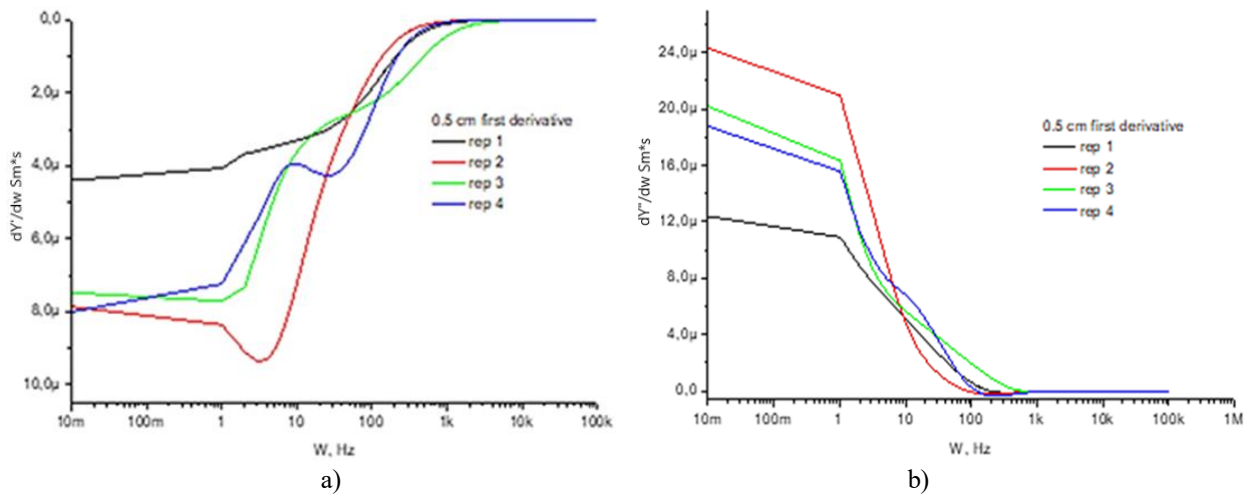


Fig. 2. Logarithmic curves of the dependence of the first derivative of the real (a) and imaginary part (b) of the conductivity of liver samples 0.5 cm in size during repeated acquisition as a function of frequency.

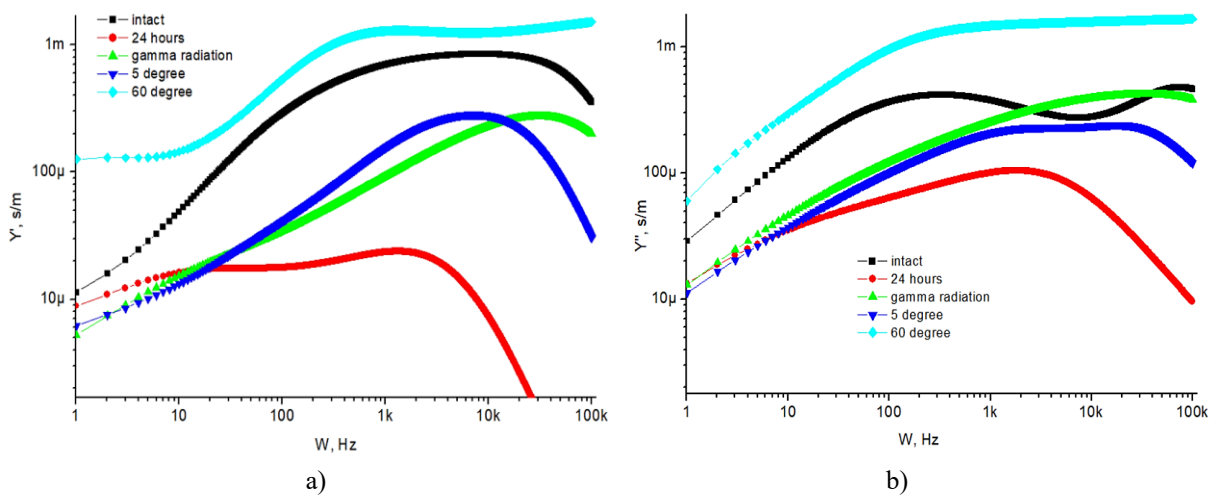


Fig. 3. Graphs of the dependence of the real (a) and imaginary part (b) of the conductivity of liver tissues under the influence of destructive factors as a function of frequency.

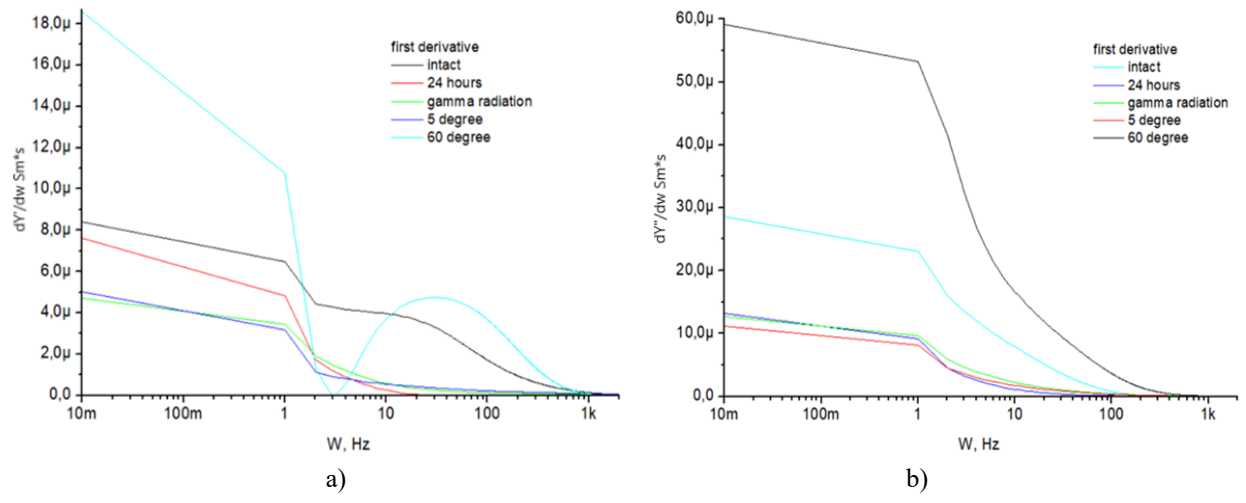


Fig. 4. Graphs of the dependence of the second first derivative of the real (a) and imaginary part (b) of the conductivity of liver samples under the influence of destructive factors as a function of frequency.

It is caused by the difference in electrical conductivity between intracellular and extracellular fluid, separated by a non-conductive (dielectric) membrane, which acts as a microscopic capacitor. In this frequency range, ions do not have time to pass through the membranes, so they accumulate on their surfaces, causing polarization effects and an increase in tissue impedance. Alpha-dispersion reflects the structural and electrical organization of cells and is sensitive to changes in their integrity. In comparison with the previous graphs, samples after exposure to destructive factors, as expected, show significant changes in frequency behavior. A decrease in real conductivity at low frequencies may be a sign of impaired cell membrane integrity and loss of conductive channels. The imaginary part becomes more chaotic, which may reflect the destruction of structures responsible for capacitive behavior.

The appearance of new maxima or their disappearance can be a clear indicator of the destruction of the tissue's internal architecture. The derivative allows localizing areas of greatest sensitivity to changes, which makes it a promising tool for quantitative analysis of the degree of damage.

Table 2. Position of local minima of the dy"/dw derivative depending on the destructive factor's influence.

| destructive factor | frequency of local minimum position, Hz | |
|--------------------|---|--|
| intact | 0,79 | |
| 24 hours | 1,12 | |
| γ-radiation | 0,89 | |
| 1 hour at 5°C | 1,22 | |
| 1 hour at 60°C | 0,88 | |

Conclusions

It has been shown that the position of the local minimum of the first derivative of the imaginary part of the specific electrical conductivity of liver tissue, located near 1 Hz (alpha-dispersion region), remains stable regardless of the sample dimensions (height). This indicates that this parameter can serve as a reliable marker of the initial (intact) state of the tissue. Under the influence of various destructive factors (e.g., temperature changes, y-irradiation, prolonged exposure to air, chemical agents like thiourea), the position of this local minimum significantly shifts. This confirms its high sensitivity to structural changes in the tissue caused by these factors. The results obtained indicate the feasibility of using the first derivative of the imaginary part of conductivity as an informative marker for diagnosing and monitoring pathological and destructive processes in biological tissues, complementing classic impedance methods. Further research is needed to deepen the understanding of the mechanisms of changes in electrical properties of tissues under the influence of destructive factors and to apply the developed approach in clinical practice.

Chervinko D.M. – PhD student;

Rachii B.I. – Doctor of Physical and Mathematical Sciences, Professor;

Yablon L.S. – Doctor of Physical and Mathematical Sciences, Professor;

Kotsiubynsky V.O. – Doctor of Physical and Mathematical Sciences, Professor;

Pakhovsky O.P. – PhD student;

Hasiuk I.M. – Doctor of Physical and Mathematical Sciences, Professor.

- [1] S. Emran, R. Lappalainen, A.M. Kullaa, & S. Myllymaa, Concentric Ring Probe for Bioimpedance Spectroscopic Measurements: Design and Ex Vivo Feasibility Testing on Pork Oral Tissues. Sensors, 18(10), 3378 (2018); https://doi.org/10.3390/s18103378.
- [2] M. Grossi, and B. Riccò, *Electrical impedance spectroscopy (EIS) for biological analysis and food characterization: a review*, J. Sens. Sens. Syst., 6, 303 (2017); https://doi.org/10.5194/jsss-6-303-2017.
- [3] Shi, Yueying & Bai, Xiaoxiao & Yang, Jingrong & Wu, Xinyu & Wang, Lei. Optimized measurement methods and systems for the dielectric properties of active biological tissues in the 10Hz-100 MHz frequency range. Frontiers in Physiology. 16 (2025); https://doi.org/10.3389/fphys.2025.1537537.
- [4] S, El. *The Use of Electrical Impedance Spectroscopy for Medical Application: A Mini Review.* Physical Science & Biophysics Journal. 7, 1 (2022); https://doi.org/10.23880/psbj-16000250.
- [5] D.A. Dean, T. Ramanathan, D. Machado, & R. Sundararajan, *Electrical Impedance Spectroscopy Study of Biological Tissues*. Journal of electrostatics, 66(3-4), 165 (2008); https://doi.org/10.1016/j.elstat.2007.11.005.
- [6] Pinto, Sandra & Pinzón, Edgar & Melendez, Angel & Mendez, Stelia & Miranda, David. *Limpieza de electrodos y reproducibilidad de medidas de impedancia eléctrica en células HeLa en solución acuosa*. Revista de la Academia Colombiana de Ciencias Exactas, Físicas y Naturales. 44, 257 (2020); https://doi.org/10.18257/raccefyn.919.
- [7] Dean, David & Thillaiyan, Ramanathan & Machado, Diego & Sundararajan, Raji. *Electrical Impedance Spectroscopy Study of Biological Tissues*. Journal of electrostatics. 66, 165 (2008); https://doi.org/10.1016/j.elstat.2007.11.005.
- [8] T. Gerasimenko, S. Nikulin, G. Zakharova, A. Poloznikov, V. Petrov, A. Baranova, & A. Tonevitsky, *Impedance Spectroscopy as a Tool for Monitoring Performance in 3D Models of Epithelial Tissues*. Frontiers in bioengineering and biotechnology, 7, 474 (2020); https://doi.org/10.3389/fbioe.2019.00474.
- [9] Van Haeverbeke, Maxime & De Baets, Bernard & Stock, Michiel. *Plant impedance spectroscopy: a review of modeling approaches and applications*. Frontiers in Plant Science. 14 (2023); https://doi.org/10.3389/fpls.2023.1187573.
- [10] Bertemes Filho, Pedro & Nogueira Cavalieri, Ricardo. *Plant tissue differentiation using electrical impedance spectroscopy with deep neural networks*, International Journal of Biosensors & Bioelectronics. 6, (2020); https://doi.org/10.15406/ijbsbe.2020.06.00182.

- [11] Yao, Jiafeng & Wang, Li & Liu, Kai & Wu, Hongtao & Jingshi, Huang & Li, Jianping. *Evaluation of Electrical Characteristics of Biological tissue with Electrical Impedance Spectroscopy*. Electrophoresis., 41(16-17), 1425 (2020); https://doi.org/10.1002/elps.201900420.
- [12] G.M.G. da Silva, P.M. Faia, S.R. Mendes, & E.S. Araújo, *A Review of Impedance Spectroscopy Technique: Applications, Modelling, and Case Study of Relative Humidity Sensors Development*. Applied Sciences, 14(13), 5754 (2024); https://doi.org/10.3390/app14135754.
- [13] H.S. Magar, R.Y.A. Hassan, & A. Mulchandani, *Electrochemical Impedance Spectroscopy (EIS): Principles, Construction, and Biosensing Applications*. Sensors, 21(19), 6578 (2021); https://doi.org/10.3390/s21196578.
- [14] Taras Pryimak, Oksana Popadynets, Ivan Gasiuk, Taras Kotyk. *Electrical impedance spectrum transformation of liver tissues under the influence of temperature*. International Journal of Engineering Research and Applications, 11(12), 1 (2021); https://doi.org/10.9790/9622-1112010111.
- [15] J. Hou, R. Strand-Amundsen, S. Hødnebø, T.I. Tønnessen, & J.O. Høgetveit, *Assessing Ischemic Injury in Human Intestine Ex Vivo with Electrical Impedance Spectroscopy*. Journal of electrical bioimpedance, 12(1), 82 (2021); https://doi.org/10.2478/joeb-2021-0011.
- [16] S.M. Abie, Ø.G. Martinsen, B. Egelandsdal, J. Hou, F. Bjerke, A. Mason, & D. Münch, *Feasibility of Using Electrical Impedance Spectroscopy for Assessing Biological Cell Damage during Freezing and Thawing*. Sensors (Basel, Switzerland), 21(12), 4129 (2021); https://doi.org/10.3390/s21124129.
- [17] S. Abasi, J.R. Aggas, G.G. Garayar-Leyva, B.K. Walther, & A. Guiseppi-Elie, *Bioelectrical Impedance Spectroscopy for Monitoring Mammalian Cells and Tissues under Different Frequency Domains: A Review*. ACS measurement science au, 2(6), 495 (2022); https://doi.org/10.1021/acsmeasuresciau.2c00033.
- [18] Y. Guo, W. Wang, W. Li, J. Li, M. Zhu, R.nSong, W. Zhu, L. Wang, Z. Ji, & X. Shi, In vivo electrical properties of the healthy liver and the hepatic tumor in a mouse model between 1 Hz and 1 MHz during a thermal treatment. International journal of hyperthermia: the official journal of European Society for Hyperthermic Oncology, North American Hyperthermia Group, 41(1), 2396122 (2024); https://doi.org/10.1080/02656736.2024.2396122.
- [19] S. Prakash, M.P. Karnes, E.K. Sequin, J.D. West, C.L. Hitchcock, S.D. Nichols, M. Bloomston, S.R. Abdel-Misih, C.R. Schmidt, E.W. Martin, S.P. Jr, Povoski, & V.V. Subramaniam, Ex vivo electrical impedance measurements on excised hepatic tissue from human patients with metastatic colorectal cancer. Physiological measurement, 36(2), 315 (2015); https://doi.org/10.1088/0967-3334/36/2/315/.
- [20] S. Fuentes-Vélez, S. Fagoonee, A. Sanginario, M. Pizzi, F.nAltruda, & D. Demarchi, *Electrical Impedance-Based Characterization of Hepatic Tissue with Early-Stage Fibrosis*. Biosensors, 12(2), 116 (2022); https://doi.org/10.3390/bios12020116.
- [21] E. Priidel, P. Annus, A. Krivošei, M. Rist, R. Land, M. Min, & O. Märtens, *Methods for Detection of Bioimpedance Variations in Resource Constrained Environments*. Sensors (Basel, Switzerland), 20(5), 1363 (2020); https://doi.org/10.3390/s20051363.
- [22] R.P. Jokhi, V.V. Ghule, B.H. Brown, & D.O. Anumba, *Reproducibility and repeatability of measuring the electrical impedance of the pregnant human cervix-the effect of probe size and applied pressure*. Biomedical engineering online, 8, 10(2009); https://doi.org/10.1186/1475-925X-8-10.
- [23] V. Garr Barry, J.L. Chiang, K.G. Bowman, K.D. Johnson, & B.A. Gower, *Bioimpedance-Derived Membrane Capacitance: Clinically Relevant Sources of Variability, Precision, and Reliability.* International journal of environmental research and public health, 20(1), 686 (2022); https://doi.org/10.3390/ijerph20010686.
- [24] S. Kophamel, L.C. Ward, E. Ariel, D. Mendez, L.M. O'Brien, L. Burchell, & S.L. Munns, *A Standardized Protocol for Measuring Bioelectrical Impedance in Green Turtles (Chelonia mydas)*. Physiological and biochemical zoology: PBZ, 96(2), 87 (2023); https://doi.org/10.1086/722451.
- [25] K. Kulkeaw, & W. Pengsart, *Progress and Challenges in the Use of a Liver-on-a-Chip for Hepatotropic Infectious Diseases.* Micromachines, 12(7), 842 (2021); https://doi.org/10.3390/mi12070842.
- [26] Grimnes, Sverre & Martinsen, Ørjan. *Alpha-dispersion in human tissue*. Journal of Physics: Conference Series. 224, 012073 (2010); https://doi.org/10.1088/1742-6596/224/1/012073.

Д.М. Червінко, Б.І. Рачій, Л.С. Яблонь, В.О. Коцюбинський, О.П. Паховський, І.М. Гасюк

Зміна форми дисперсійної кривої провідності тканини печінки під впливом деструктивних факторів

Прикарпатський національний університет імені Василя Стефаника, Кафедра прикладної фізики та матеріалознавства, Івано-Франківськ, Україна, <u>ivan.hasiuk@pnu.edu.ua</u>

У роботі досліджується частотна дисперсія електричних властивостей біологічних тканин, зокрема печінки свині, за допомогою спектрального аналізу провідності. Чисельне диференціювання імпедансних характеристик було застосовано в широкому діапазоні частот $(0,01\ \Gamma \eta-100\ \kappa\Gamma \eta)$ для виявлення локальних переходів між електрофізіологічними режимами тканин. Показано, що положення локального мінімуму першої похідної уявної частини питомої провідності поблизу $1\ \Gamma \eta$, що відповідає альфа-дисперсії та міжфазній поляризації на клітинних мембранах, залишається стабільним незалежно від розміру зразка, але чутливо зміщується під впливом деструктивних факторів (наприклад, температури, радіації). Ці результати підтверджують можливість використання похідних провідності як інформативного маркера структурних змін у тканинах, що доповнює класичні імпедансні підходи для діагностики та моніторингу патологічних процесів.

Ключові слова: імпедансна спектроскопія, дисперсія електропровідності, тканини печінки, схема електричного еквівалента, руйнування, альфа-дисперсія, числове диференціювання, біологічні тканини, клітинні мембрани.